

RESEARCH ARTICLE

10.1029/2018JB017062

Key Points:

- Poroelastic stress changes favor fault reactivation in basement in normal and strike-slip faulting regimes for conduit-barrier faults
- Sealing normal fault and reduced material contrast between reservoir and basement favor reactivation in reservoir over basement
- Direct pore pressure effects prevail over poroelastic stress in increasing Coulomb failure stress but are insufficient to lead to basement fault reactivation

Supporting Information:

- Supporting Information S1

Correspondence to:

P. Eichhubl,
peter.eichhubl@beg.utexas.edu

Citation:

Fan, Z., Eichhubl, P., & Newell, P. (2019). Basement fault reactivation by fluid injection into sedimentary reservoirs: Poroelastic effects. *Journal of Geophysical Research: Solid Earth*, 124, 7354–7369. <https://doi.org/10.1029/2018JB017062>

Received 19 NOV 2018

Accepted 7 JUN 2019

Accepted article online 19 JUN 2019

Published online 22 JUL 2019

Basement Fault Reactivation by Fluid Injection Into Sedimentary Reservoirs: Poroelastic Effects

Zhiqiang Fan^{1,2} , Peter Eichhubl¹ , and Pania Newell^{3,4}

¹Bureau of Economic Geology, Jackson School of Geosciences, The University of Texas at Austin, Austin, TX, USA, ²Now at Desert Research Institute, Reno, NV, USA, ³Sandia National Laboratories, Albuquerque, NM, USA, ⁴Now at Department of Mechanical Engineering, University of Utah, Salt Lake City, UT, USA

Abstract To investigate mechanisms of seismic fault reactivation in crystalline basement in response to fluid injection in overlying sedimentary reservoirs, we conducted three-dimensional finite element simulations to assess the effects of direct pore pressure communication and indirect poroelastic stress transfer on the change in Coulomb failure stress of favorably oriented faults of varying permeability structure in normal, strike-slip, and reverse faulting stress regimes. We demonstrate that the direct pore pressure effect transmitted along a hydraulically conductive fault exceeds the indirect poroelastic effect, but alone is insufficient for fault reactivation in the basement. The poroelastic effect on the Coulomb failure stress results from induced normal tractions and, to a lesser extent, from induced shear tractions that relate to the flexing of the fault as the reservoir expands poroelastically with fluid injection. Assuming a higher Biot coefficient for reservoir over basement rock as previously reported, the combined direct pore pressure and indirect poroelastic effects result in reactivation of hydraulically conductive faults in the basement in normal and strike-slip faulting stress regimes and in the reservoir in reverse faulting regimes. Sealing normal faults that are not preferentially conductive also preferentially reactivate in the reservoir. These findings apply to injection in either hanging or footwall of normal and reverse faults. Reducing the contrast in Biot coefficient between reservoir and basement favors fault reactivation in the reservoir for injection in the footwall in normal faulting stress regimes. These simulations demonstrate that geomechanical models without coupled poroelasticity underestimate the potential of fault reactivation in crystalline basement.

1. Introduction

Wastewater associated with oil and gas operations including formation brine and recovered hydraulic fracturing fluids is routinely disposed of through reinjection into formations of high porosity and permeability. The recently observed increase in earthquake activity in a number of states has been linked to high-volume wastewater disposal in conjunction with oil and gas production from low-permeability unconventional reservoirs, with numerous reports documenting or inferring seismic events along faults in basement that underlies the sedimentary disposal reservoirs (Barbour et al., 2017; Horton, 2012; Keranen et al., 2013; Kim, 2013; Langenbruch et al., 2018; Nicholson & Wesson, 1990; Seeber et al., 2004; Seeber & Armbruster, 1993; Walsh & Zoback, 2015; Yeck et al., 2016). Although the depth of seismic events, in particular events early within a seismic sequence prior to deployment of local stations, may be uncertain and may follow complex patterns of basement and sediment hosted activity at any given location, seismic reactivation of basement faults in areas of active wastewater injection can be considered common (Ogwari et al., 2016; Walsh & Zoback, 2015; Yeck et al., 2016). Yet, the physical processes that potentially allow faults in basement to reactivate in response to wastewater disposal by injection in the overlying sedimentary units are uncertain.

Two fundamental physical processes have been proposed to account for basement fault reactivation: direct pressure transfer from the reservoir to the basement, possibly enabled by preferential flow along hydraulically conductive faults (Ellsworth, 2013; Hornbach et al., 2015; Langenbruch et al., 2018; Ogwari et al., 2018; Zhang et al., 2013) and poroelastic strain transfer from the reservoir to the basement (Barbour et al., 2017; Chang & Segall, 2016a, 2016b; Segall & Lu, 2015). In addition, stress transfer from slip on shallow faults to basement faults has been invoked to account for basement fault reactivation (Keranen et al., 2013) but would, by itself, not account for the widespread occurrence of basement fault seismicity. In this study, we focus on the first two processes. Among coupled flow-geomechanics simulations that consider poroelastic effects, Rutqvist et al. (2007) and Cappa and Rutqvist (2011) did not account for deviations of the Biot

coefficient from 1. Barbour et al. (2017) and Zhai and Shirzaei (2018) simulated poroelastic effects of injection into a layered elastic half-space without including the effect of faults on pressure diffusion. Chang and Segall (2016a, 2016b) simulated poroelastic effects on basement fault reactivation and seismicity rate using a multilayered two-dimensional plane strain model for a normal fault. The separate contributions to changes in Coulomb failure stress (CFS) from direct pore pressure increase and resulting poroelastic stress were quantified. They demonstrated that earthquakes can occur in the basement along normal faults that are either isolated or connected to the reservoir. They simulated the effect of both conduit and sealing faults, but in either case, the faults do not extend across the reservoir layer. Therefore, their sealing faults do not affect the pressure distribution in the reservoir potentially underestimating the pressure disturbance and fault reactivation potential in the reservoir. In contrast to their models, we extend the faults across the reservoir. Because of the common occurrence of fault zones with a conduit-barrier permeability structure and their strong hydraulic anisotropy, with cross-fault permeability potentially orders of magnitude lower than fault-parallel permeability (Bense et al., 2013; Caine et al., 1996), we also simulate the effects of combined conduit-barrier fault permeability structure that enhances flow along the fault into the basement within a conductive fault damage zone while preventing flow across the low-permeability fault core. Extending the conduit-barrier fault across the reservoir potentially increases the excess pore pressure and fault reactivation potential in the reservoir. A conduit-barrier fault extending from the basement into the reservoir may thus provide the highest reactivation potential for faults in basement. Using three-dimensional numerical simulations, we also simulate the effects of fluid injection on optimally oriented reverse and strike-slip faults and investigate the effect of injecting into the footwall versus hanging wall of dipping faults as fluid injection into footwall or hanging wall is widely reported (Jeanne et al., 2018; Konstantinovskaya et al., 2014). Compared to two-dimensional simulations, the three-dimensional approach correctly accounts for out-of-plane pressure diffusion and poroelastic strains, resulting in a better estimate of changes in vertical displacement that are overestimated in plane-strain analysis. In addition, examples of reported basement seismicity linked to wastewater injection into sedimentary units in strike-slip faulting stress regimes (Kim, 2013; Nicholson et al., 1988; Seeber et al., 2004) necessitate three-dimensional simulations that consider all three Andersonian stress regimes: normal, reverse, and strike-slip. Stress regime also influences fluid diffusion (Johann et al., 2016) and the poroelastic response of the reservoir, potentially affecting basement fault reactivation. While Chang and Segall (2016a, 2016b) simulated the rate of seismicity within the basement using rate- and state-dependent friction, we aim at answering the question if reactivation of a favorably oriented fault can occur in the basement before reactivation of the same fault in the overlying reservoir. We address the question of basement versus sediment fault reactivation for all three Andersonian stress regimes and as a function of fault permeability structure.

We use the CFS to assess fault reactivation potential, defined for a cohesionless fault as

$$\text{CFS} = \tau - \mu (\sigma_n - p), \quad (1)$$

where μ is the coefficient of friction, p is pore fluid pressure, and τ and σ_n are shear and total normal tractions acting on the fault, respectively. A positive CFS is taken here to indicate fault reactivation (compression positive). We note that this criterion addresses fault stability without distinguishing if slip is seismic or aseismic. During fluid injection, pore pressure dissipates away from the wellbore by fluid migration within the reservoir and possibly along a permeable fault damage zone into the basement, resulting in an excess pore pressure Δp that will generally be higher in the injection reservoir compared to the basement. We define the excess pressure by $\Delta p = p - p_i$, where p_i is the pressure prior to injection. While p_i can be of any magnitude, we assume that the pressure depth gradient within the injection reservoir and the basement is hydrostatic prior to injection. After injection, as Δp generally decreases with distance from the injection well, excess pressure will be higher in the reservoir than in the basement, thus favoring fault reactivation in the reservoir. Therefore, the distribution of excess pore pressure alone cannot generally account for the nucleation of seismicity in crystalline basement induced by injection in overlying sedimentary formations. Although rupture nucleation in the basement can, in principle, be attributed to differences in fault frictional or hydraulic properties between basement and reservoir, we investigate here if poroelastic stress changes can account for basement fault reactivation for faults of uniform frictional and hydraulic properties along dip. Generally, fluid injection into reservoirs affects stability of basement faults via two coupled processes: (1) raising pore pressure thus decreasing the effective normal stress and lowering the resistance to fault

Table 1
Mechanical and Hydraulic Rock Properties

Hydromechanical property	Overburden	Caprock	Reservoir	Basement
Top from surface (m)	0	1,500	1,600	1,750
Young's modulus (GPa)	14.4	10	14.4	37.5
Poisson's ratio	0.2	0.15	0.2	0.25
Biot coefficient	0.79	0.7	0.79 ^a	0.44
Skempton coefficient	0.62	0.8	0.62 ^b	0.46
Porosity (percent)	15	10	15	5
Permeability (mDarcy)	200	1E-5	100	1E-4
Diffusivity (m ² /s)	1.64	7.8E-8	0.82	2.83E-6

^a0.44 in section 3.4. ^b0.46 in section 3.4.

reactivation (direct pressure effect) and (2) changing the shear and normal tractions acting on the fault because of poroelastic stress changes.

We assume that porous fluid flow follows Darcy's law and the fluid-saturated reservoir and basement rocks follow classical Biot poroelasticity. Poroelasticity is a natural extension of classical elasticity to incorporate the two-way coupling between rock deformation and fluid flow (Wang, 2000). For an isotropic fluid-saturated poroelastic medium, the constitutive relations that express the strain ϵ_{ij} and the increment of fluid content ζ in terms of the total stress σ_{ij} and the pore pressure p are given by

$$\epsilon_{ij} = \frac{1 + \nu}{E} \sigma_{ij} - \frac{\nu}{E} \sigma_{kk} \delta_{ij} + \frac{\alpha p}{3K} \delta_{ij}, \quad (2)$$

$$\zeta = \frac{\alpha}{KB} \left(\frac{B \sigma_{kk}}{3} + p \right), \quad (3)$$

where σ_{kk} is the bulk stress and δ_{ij} is the Kronecker delta. The material constants given above are as follows: Young's modulus E , the drained Poisson's ratio ν , the bulk modulus of fluid-saturated rock K , the Biot coefficient α , and Skempton's coefficient B . The Biot coefficient α is defined as $\alpha = 1 - K/K_s$, where K_s is the bulk modulus of the grains. The Biot coefficient ranges between porosity and 1 and characterizes the efficiency of pore fluid in counteracting to the total applied stress. The Skempton coefficient B is the ratio of induced pore pressure to the change in applied pressure in undrained conditions. The strength of poroelastic coupling is the product of Biot coefficient and Skempton coefficient (Zimmerman, 2000).

The magnitude of induced poroelastic stress by fluid injection is mainly controlled by the products of Biot coefficient and Skempton coefficient. Compared with sedimentary injection strata, crystalline basement rocks generally have negligible porosity and higher stiffness, hence a lower Biot coefficient α , with representative values of 0.3–0.7 for granite and 0.6–0.9 for sandstone (Paterson & Wong, 2005; Tan et al., 2015; Wang, 2000). Intermediate values of 0.44 and 0.79 for basement and sediment, respectively, are used in this study for the base case simulations (Table 1). A higher Biot coefficient in the sediment would result in a more pronounced poroelastic coupling effect in the reservoir than in the basement. The magnitude of induced poroelastic stress has a direct effect on fault reactivation as can be seen from equation (1). We note that the effect of reservoir stiffness on fault reactivation is fully captured via indirect poroelastic deformation, as indicated from equation (2).

A quantitative understanding of poroelastic stress changes in response to injection, and the differences in these effects for reservoir and basement lithology, can be gained from the three-dimensional numerical simulations of transient pore pressure and poroelastic stress in the fault zone associated with fluid injection as shown in the next section. In the following, we simulate the coupled pore pressure and stress evolution for the three Andersonian stress regimes to quantify the conditions under which basement fault reactivation can occur.

2. Methods

We simulate the spatial and temporal distribution of pore pressure and stress in the vicinity of the injector and the basement fault using three-dimensional Abaqus finite element models (ABAQUS, 2014). The

modeling domain extends vertically from the surface to a depth of 6 km and horizontally to 8 km \times 16 km (Figure 1). With the injector located at the edge of the model domain, and using symmetry considerations, the model represents a three-dimensional space of 6 km \times 16 km \times 16 km. Simulations for an extended domain size of 6 km \times 100 km \times 100 km are summarized in the supporting information. The differences in results between the two domain sizes are small enough to allow use of the computationally more efficient smaller domain for the purpose of this study. The model consists of four layers: the 150-m-thick reservoir is situated between basement and a 100-m-thick caprock layer which is overlain by 1,500 m of overburden. In all models, a fault cuts across the basement and penetrates into the overlying reservoir. The width of the fault is assumed to be 20 m, consisting of a 4-m-thick, low-permeability core ($k = 1\text{E-}5$ mD) bounded by two 8-m-thick damage zones ($k=100$ mD). The distance between the injection well and the upper tip of the fault is 1 km. The mechanical and hydraulic properties for each layer are listed in Table 1. For the base case, the fault is represented as a combined flow conduit-barrier system (Caine et al., 1996), acting as barrier for flow across a low-permeability fault core and as a preferred conduit for flow parallel to the fault in the fault damage zone that surrounds the fault core. The fault has the same mechanical properties as the host rock units that it transects. We also consider the cases of a sealing fault without conductive damage zone and of a conduit fault composed of the conductive damage zone but without the fault core that limits flow across the fault. Based on laboratory data summarized by Wang (2000) and Paterson and Wong (2005), we initially assume that the reservoir rock has larger Biot and Skempton coefficients and a smaller Poisson's ratio than the basement (Table 1) and assess the effect of differences in poroelastic properties in section 3.4.

We simulate the effects of continuous injection of water into the reservoir over 10 years at a constant injection rate of 60,000 m³/month, a common injection rate for wastewater disposal in Texas (Frohlich et al., 2014; Hornbach et al., 2015). The total number of brick elements (C3D20P elements in Abaqus) is 75,816, with a refined mesh in the vicinity of the injection well and in and around the fault zone (Figure 2). Each element has 20 nodes that are equipped with displacement and pore pressure degrees of freedom.

Normal displacements at the lateral boundaries and bottom surface are zero. The top surface is traction free. Drained conditions are applied to all boundaries except the front surface, which contains the injection well and is treated as a symmetry plane. The initial pore pressure is hydrostatic with a gradient of 10.3 MPa/km. Fluid viscosity is 1.11E-3 Pa s (Hornbach et al., 2015). We consider the three Andersonian stress regimes: normal faulting ($\sigma_v \geq \sigma_{Hmax} \geq \sigma_{hmin}$), reverse faulting ($\sigma_{Hmax} \geq \sigma_{hmin} \geq \sigma_v$), and strike-slip faulting ($\sigma_{Hmax} \geq \sigma_v \geq \sigma_{hmin}$), where σ_v is the vertical stress and σ_{hmin} and σ_{Hmax} are the minimum and maximum principal horizontal in situ stresses, respectively. Stress conditions and fault orientation are summarized in Table 2. The initial stress state allows the fault to be optimally oriented for slip and below the magnitude necessary for fault reactivation.

Although thermal stresses stemming from the injection of cold water into the reservoir can affect the stress state near the wellbore, the injected water is likely to be thermally equilibrated once it reaches the vicinity of the fault. Thermal stresses are therefore not accounted for in these simulations for computational efficiency.

3. Results

3.1. Conduit-Barrier Fault, Injection in the Hanging Wall

We first examine the effect of stress regime on the spatial and temporal evolution of stress and pore pressure on the fault with conduit-barrier flow properties. The normal and reverse faults are assumed to dip toward the injector, that is, injection occurs in the hanging wall (Figures 1a and 1b). The excess pore pressure profile after 10 years of continuous water injection is shown in Figures 2a–2c for the normal faulting, reverse faulting, and strike-slip faulting stress regimes, respectively. The maximum pore pressure change at the bottom of injection well is about 5 MPa after 10 years of continuous injection. The pore pressure anomaly continues to expand radially until it reaches the fault where the high-permeability fault damage zone allows the pore pressure to propagate downward from the reservoir into the basement. In addition, the low-permeability fault core serves as a barrier to flow across the fault creating a pore pressure discontinuity across the fault.

The excess pore-pressure and CFS evolution are tracked for three points that are located along the fault on the side of the fault facing the injector (upstream side; Figures 1a–1c), with point A located within the reservoir, point B within the basement 25 m below the reservoir layer, and point C deeper in the basement 1,900

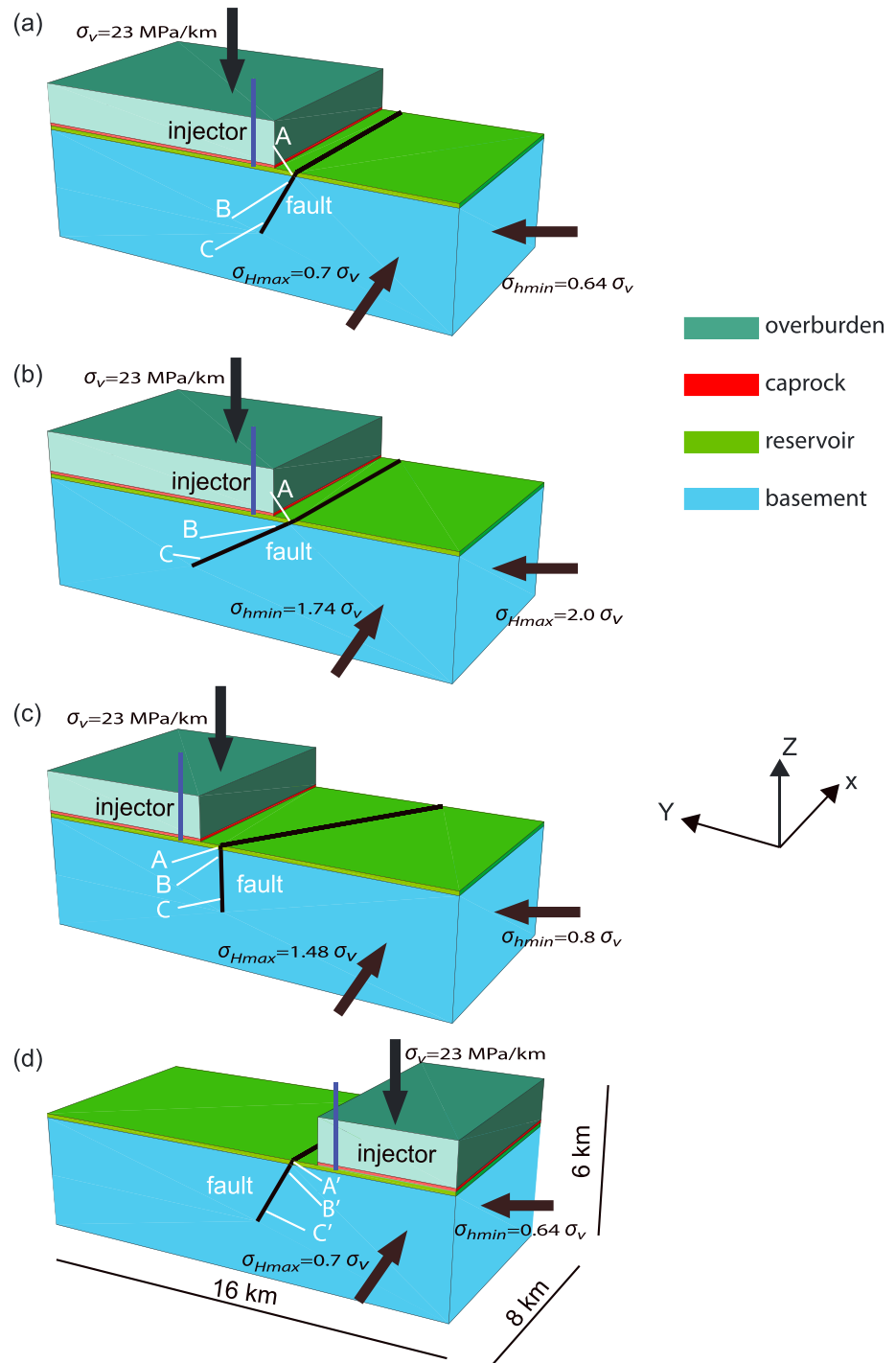


Figure 1. Fault and layer geometry and in situ stress conditions for finite element simulations. Overburden (dark green) above injection reservoir (light green) is partially removed to display fault geometry. The fault extends from the basement (blue) across the reservoir and terminates against the caprock (red). Coulomb failure stress on the fault is tracked at points A (A') located within the reservoir, at point B (B') in the basement immediately below the reservoir, and at C (C') deep in the basement. (a) Normal faulting stress regime, injection into hanging wall. (b) Reverse faulting stress regime, injection into hanging wall. (c) Strike-slip faulting stress regime. (d) Normal faulting stress regime, injection into the footwall.

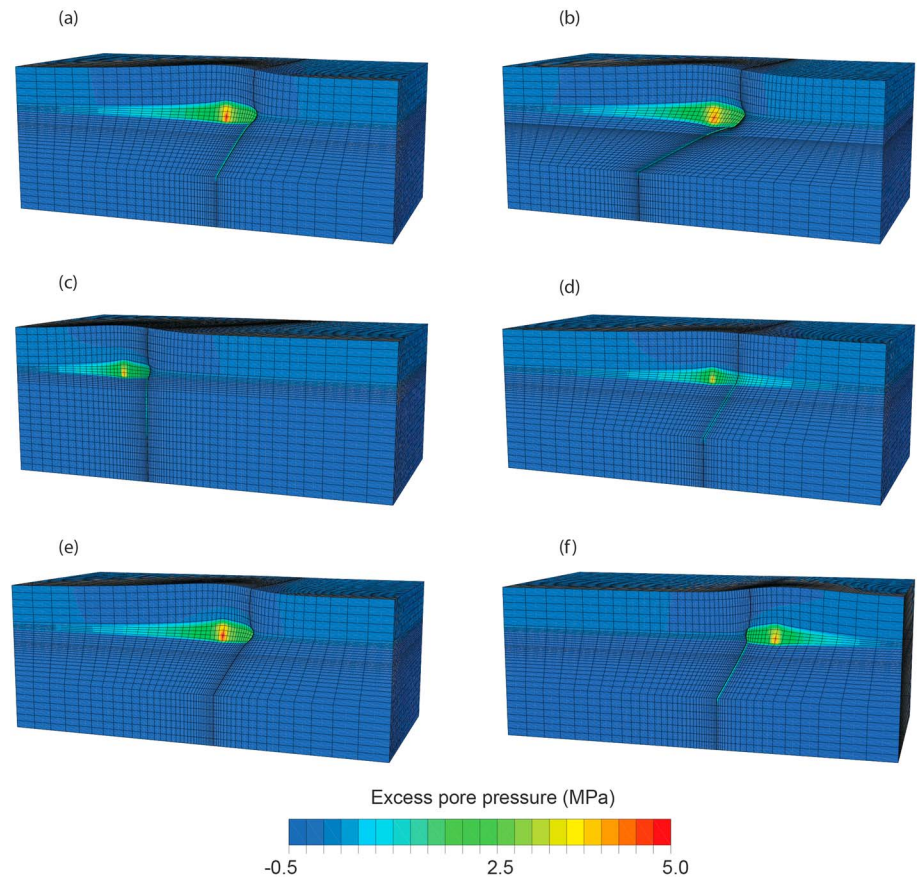


Figure 2. Excess pore pressure profile after 10 years of continuous injection for a conduit-barrier fault in (a) normal faulting, (b) reverse faulting, (c) strike-slip faulting stress regimes, (d) a conduit fault in normal faulting stress regime, and (e) a sealing fault in normal faulting stress regime. Injection for (a)–(e) on the left side (hanging wall). (f) Conduit-barrier fault in normal faulting stress regime with fluid injection into the footwall. Displacement induced by volumetric expansion of the reservoir is shown not to scale.

m below the reservoir layer. The simulated excess pore pressure and CFS, plotted in Figures 3a–3f for the three stress regimes, increase monotonically with time and follow a similar trend. Note that the initial differential stress and CFS increase from the normal to the strike-slip and to the reverse faulting stress regime. At point C, the lower basement observation point, the differential stress prior to injection is already large especially for the reverse faulting stress regime. Poroelastic stress changes do not affect the CFS and thus the stability of the fault significantly at point C, and CFS remains negative (Figures 3a–3f). Therefore, in the following analysis, we focus on stress and pore pressure changes at points A and B. For the normal and strike-slip faulting stress regime, the initial CFS prior to injection along the upper basement segment of the fault (point B) is smaller than that at point A located in the reservoir (Figures 3b and 3d). However, CFS at point B increases at a faster rate than that at point A and becomes positive earlier in the injection history (see inserts in Figures 3b and 3f), thus allowing fault reactivation in the

Table 2
Stress Conditions and Fault Orientation

Stress regime	σ_v (MPa/km)	σ_{Hmax} (MPa/km)	σ_{hmin} (MPa/km)	Fault dip	Fault strike
Normal faulting	23	16	14.7	60°	Parallel to σ_{Hmax}
Reverse faulting	23	46	40	30°	Parallel to σ_{hmin}
Strike-slip faulting	23	34	18.4	90°	30° to σ_{Hmax}

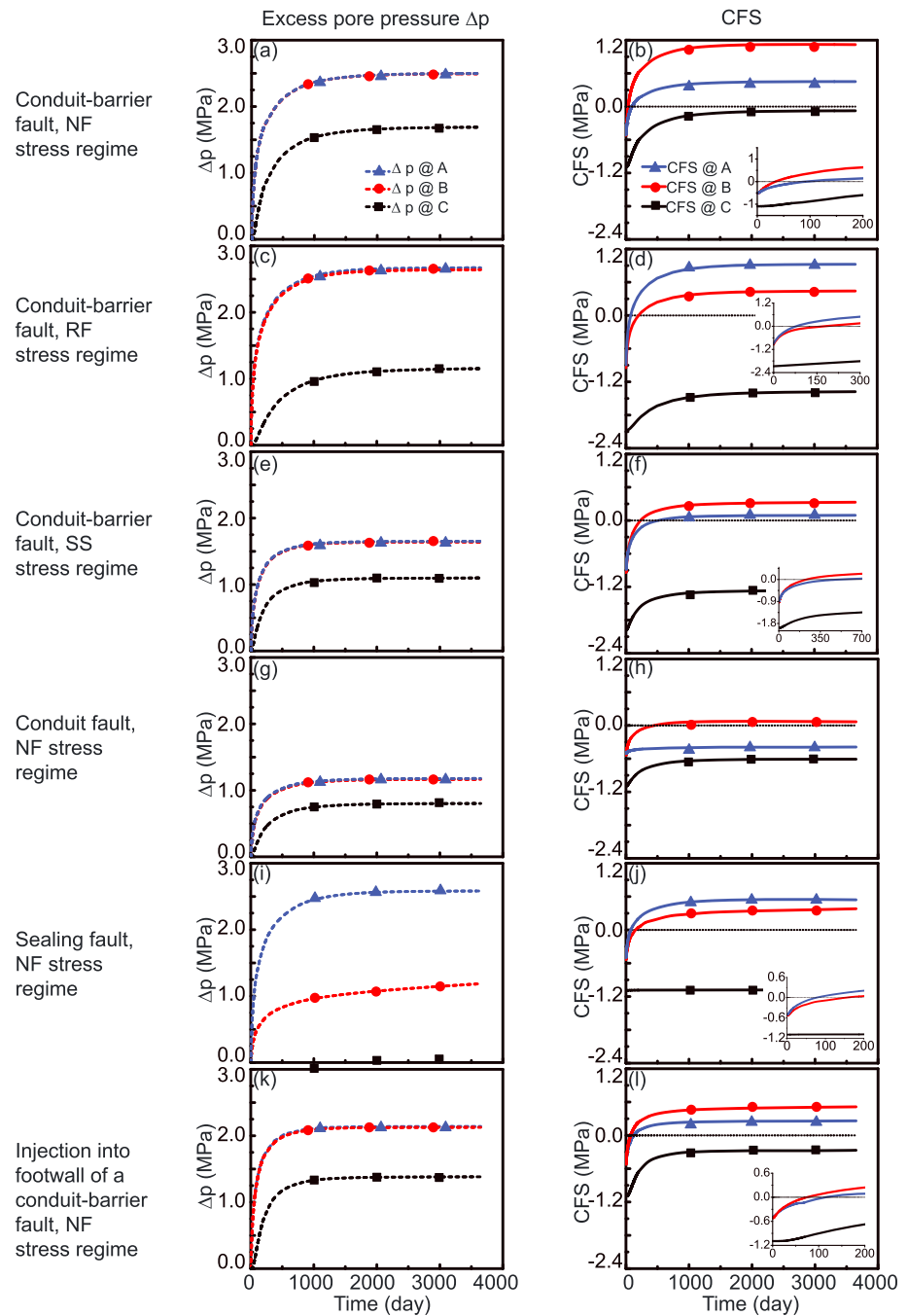


Figure 3. Evolution of excess pore pressure Δp (left column) and Coulomb failure stress (CFS; right column) at points A, B, and C along the fault. The inserts show the evolution of CFS over the first few hundred days to illustrate if fault reactivation is favored in the upper basement or not. Injection into a conduit-barrier fault in a normal (NF; a, b), reverse (RF; c, d), and strike-slip faulting (SS; e, f) stress regime. Injection into a conduit fault in a normal faulting stress regime (g, h). Injection into a sealing fault in a normal faulting stress regime (i, j). Injection into footwall of a conduit-barrier fault in a normal faulting stress regime (k, l).

shallow basement at point B before point A located in the reservoir despite excess pore pressures being nearly identical at both points. We attribute this behavior to poroelastic stress changes.

The contribution of the direct pore pressure increase to the increase in CFS (ΔCFS) is equal to $\mu\Delta p$. The increase of CFS due to the poroelastic stress is $\Delta\tau - \mu\Delta\sigma_n$. Figures 4a–4f plot the individual contributions of

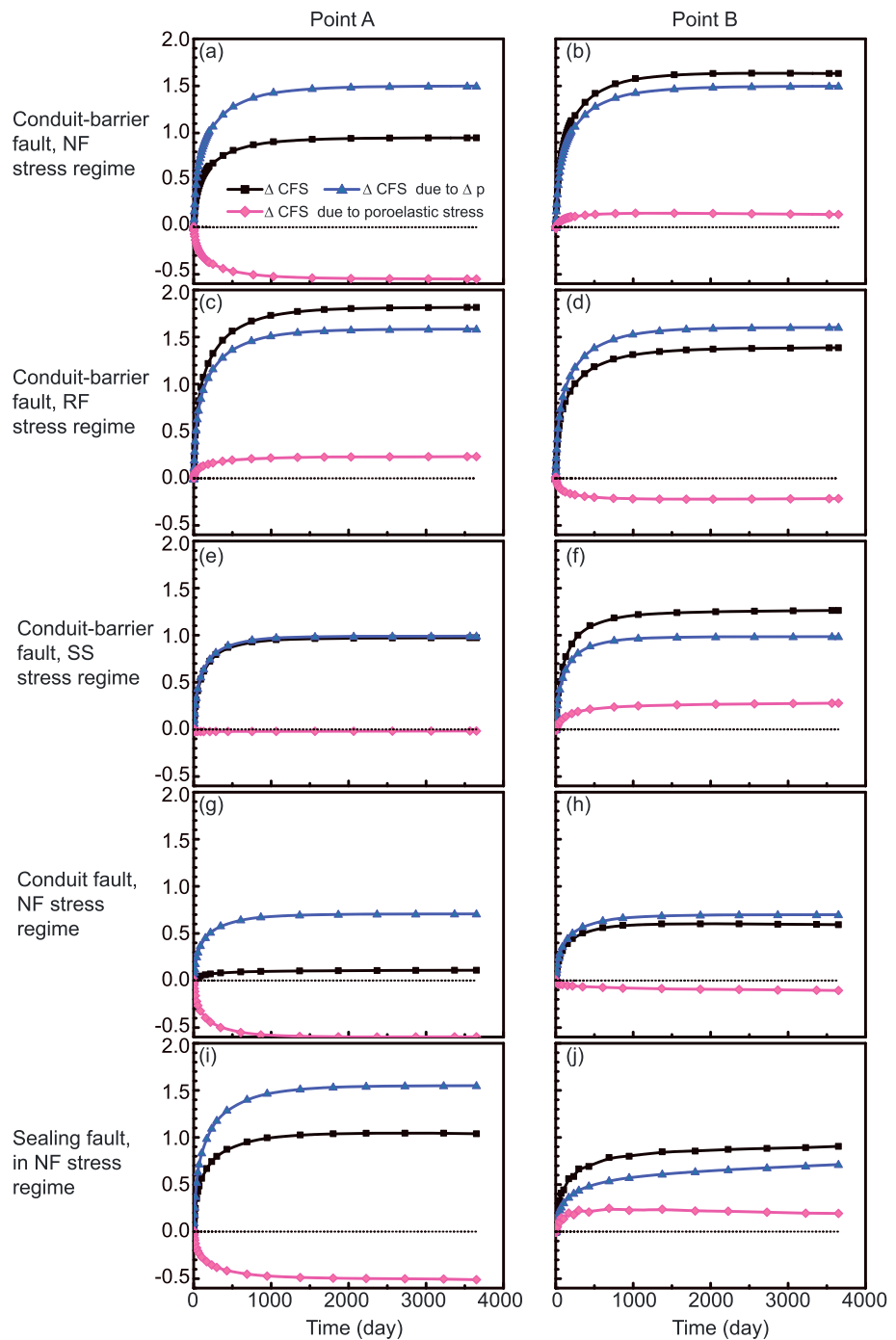


Figure 4. Change in Coulomb failure stress (CFS) in response to direct pore pressure increase and poroelastic stress at points A (left column) and B (right column). (a, b) Conduit-barrier fault in a normal faulting (NF) stress regime. (c, d) Conduit-barrier fault in a reverse faulting (RF) stress regime. (e, f) Conduit-barrier fault in a strike-slip faulting (SS) stress regime. (g, h) Conduit fault in a normal faulting stress regime. (i, j) Sealing fault in a normal faulting stress regime.

direct pore pressure increase and poroelastic stress change to the change in CFS for a friction coefficient of 0.6. Increasing the pore pressure associated with fluid injection causes a volumetric expansion in the perturbed part of the reservoir, which displaces the surrounding rocks away from the injector and induces flexing of the fault (Figures 2a–2c).

Irrespective of stress regime, the induced normal traction on the fault close to the injector stemming from the pore pressure increase and the resulting poroelastic effect are always positive (more compressive) resulting in a decrease in CFS (line marked “ ΔCFS due to $\Delta\sigma_n$ ” in Figure 4a). This induced normal traction is counteracted by the increase in pore pressure. Because the reservoir rock is simulated with a larger Biot coefficient and a smaller Poisson's ratio than the basement (Table 1), the increase in pore pressure leads to a more pronounced poroelastic effect in the reservoir as predicted by the expression

$$\frac{\Delta\sigma_{\text{hmin}}}{\Delta p} = \frac{\Delta\sigma_{\text{Hmax}}}{\Delta p} = \alpha \frac{1-2\nu}{1-\nu} \quad (4)$$

(Engelder, 1993; Segall & Fitzgerald, 1998). The induced normal traction on the fault is thus larger in the reservoir than in the basement (Figure 4a) inhibiting slip in the reservoir and favoring slip in the basement.

Flexure of the fault resulting from the volumetric expansion of the reservoir in the vicinity of the injection well (Figures 2a–2c) induces shear tractions on the fault that act in addition to the ambient or tectonic shear stress. For the normal faulting stress regime, when fluid is injected into the hanging wall of the fault, the induced shear tractions acting on the fault *below* the injection horizon increase the original shear tractions in the dip slip direction. Hence, they increase the CFS and favor basement fault reactivation. *Above* the injection horizon, the induced shear tractions on the fault are opposite in sign and act to impede reservoir fault reactivation. Additional shear tractions act within the damage zone of the basement fault resulting from the high pore pressure gradient along the downdip direction in the narrow fault damage zone that is confined between the low-permeability fault core and basement host rock. This pore pressure gradient is equivalent to a vertical body force (Wang, 2000) and induces additional shear tractions that favor normal slip on the fault.

For the reverse faulting stress regime, when fluid is injected into the hanging wall of the fault, the induced shear tractions caused by fault flexing and by the pore pressure gradient in the basement fault damage zone reduce the shear tractions and thus inhibit basement fault reactivation (Figure 4d). For the strike-slip faulting stress regime, the induced shear tractions increase the CFS in the compressional quadrant of the fault facing the injection well and in the tensional quadrant facing away from the injection well and decrease the CFS in the other two quadrants of the fault. These changes affect the fault in both the reservoir and basement. However, the induced *normal* tractions are larger in the reservoir segment of the strike-slip fault than in the basement because of the stronger stress-pore pressure coupling in the reservoir. Consequently, CFS increases along the basement segment of the fault at a higher rate than in the reservoir, thus favoring slip in the basement over the reservoir for strike-slip stress regimes (Figure 4f).

3.2. Conduit and Sealing Faults, Injection in the Hanging Wall

To assess the sensitivity of fault reactivation potential to fault permeability structure, we simulate the evolution of pore pressure and CFS over time for conduit ($k = 100$ mD) and sealing faults ($k = 1\text{E-}5$ mD) in the normal faulting stress regime (Figures 2d and 2e). All other model parameters are those used in section 3.1 and listed in Table 1. For the case of a conduit fault, the evolution of pore pressure and CFS (Figures 3g and 3h) follows similar patterns to those for a conduit-barrier fault case (Figures 3a and 3b) except that the excess pore pressure is significantly lower since cross-fault flow is allowed. Fault reactivation is therefore delayed by a few months. The flexing of the conduit fault caused by volume expansion of the reservoir is less pronounced than that for a conduit-barrier fault (Figure 2d) because the pore pressure increase on the downstream (footwall) side of the fault largely counteracts the pore pressure increase on the upstream side (hanging wall). Fault reactivation is still favored in the basement (Point B) over the reservoir portion of the fault (Point A; Figure 3h), similar to the conduit-barrier fault (Figure 3b).

Compared to the conduit-barrier fault, the sealing fault leads to a slightly higher pore pressure which is now confined to the reservoir around the injector because pressure migration from the reservoir into the basement is impeded (Figure 2e). As a result, a much higher excess pore pressure is induced in the reservoir than in the basement, and fault reactivation is favored in the reservoir. Also, the sealing fault reactivates in the reservoir later (Figure 3j) than the conduit-barrier fault reactivates in the basement (Figure 3b). The contrast in fault reactivation potential between the conduit-barrier fault and the sealing fault highlights the importance of fault permeability characterization for fault reactivation potential.

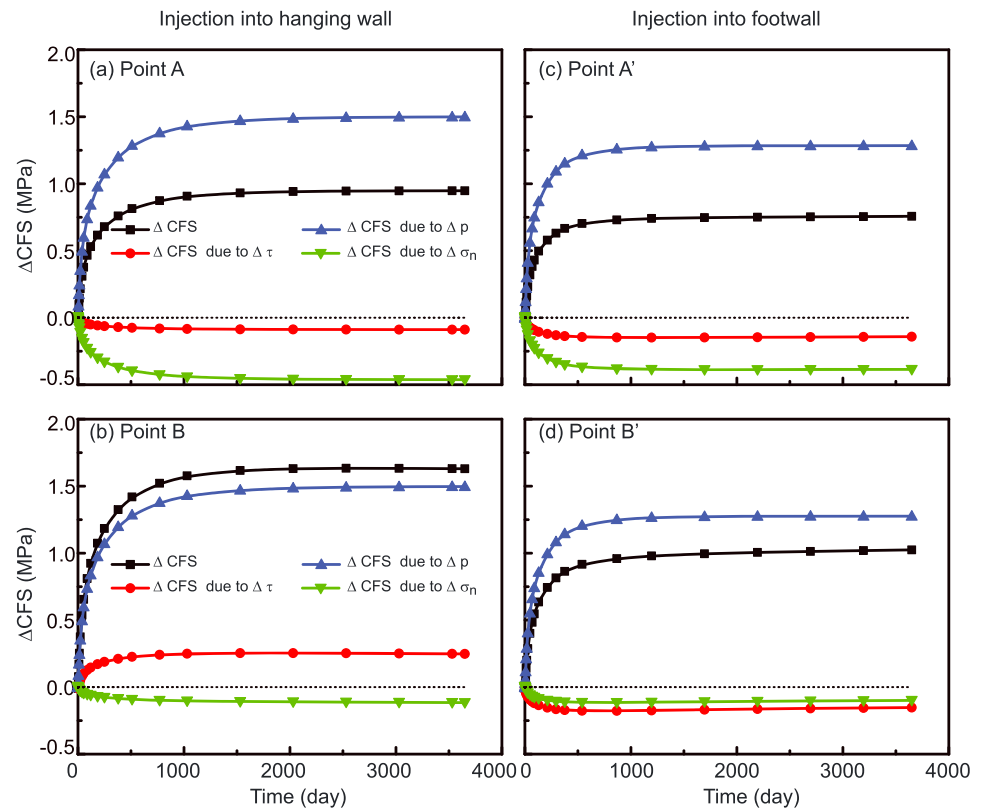


Figure 5. Changes in CFS due to changes in p , τ , and σ_n for injection into the hanging wall (left column, a, b)/footwall (right column, c, d) of a conduit-barrier fault in a normal faulting stress regime. CFS = Coulomb failure stress.

The contributions of excess pressure Δp and poroelastic stress to CFS for the conduit fault and sealing fault are shown in Figures 4g–4j (for the normal faulting stress regime) and tabulated in Table S2 (supporting information; for all 17 simulated scenarios).

3.3. Conduit-Barrier Fault, Injection in the Footwall

So far, we simulated injection into the hanging wall of normal and reverse faults. For comparison, we now consider fluid injection into the footwall but limit the discussion to the conduit-barrier normal fault (Figure 2f). The distance between the upper tip of the fault and the injector is set to 1,000 m. We track the evolution of pore pressure and CFS at three points A', B', and C' along the side of the fault facing the injector, adjacent to points A, B, and C on the hanging wall of the fault, respectively (Figures 1d, 3k, and 3l). In contrast to injection in the hanging wall where induced shear stress along the fault segment in the upper basement (point B) caused by reservoir poroelastic expansion acts in addition to the tectonic shear stress on the fault (Figure 5b), induced shear stress for injection in the footwall acts against the tectonic shear stress (Figure 5d). However, although the induced shear stress at points A' and B' is similar, the induced changes in normal stress at A' are higher than at B', resulting in a higher CFS at point B' compared to A' (Figures 5c and 5d). Therefore, similar to injection in the hanging wall for a conduit-barrier fault, injection in the footwall favors fault reactivation in the upper part of the basement before reactivation in the reservoir (Figure 3l).

Compared to injection in the hanging wall of a fault dipping toward the injector, fluid injection into the footwall of a fault dipping away from the injector results in a longer distance between well and fault, thus leading to a lower excess pressure Δp at the fault for footwall injection (Figure 3k) compared to hanging wall injection (Figure 3a). This lower excess pressure translates to a delayed fault reactivation for footwall injection compared to hanging wall injection.

The results for injection into either the hanging wall or footwall, for all three stress regimes, and for all three fault hydraulic properties are summarized in Figure 6. This figure includes the findings of simulations for

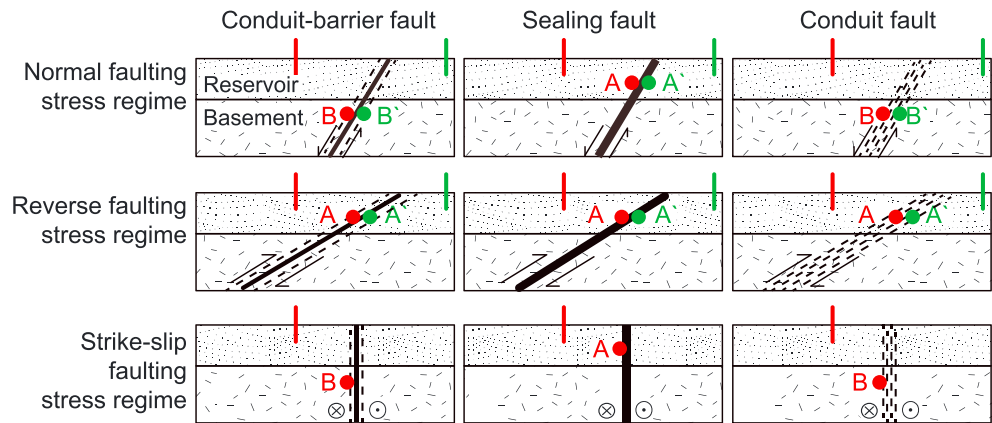


Figure 6. Location of fault reactivation relative to position of injector for an optimally oriented fault in normal, reverse, and strike-slip stress regimes and for a conduit-barrier, conduit, and sealing fault permeability structure. Fault reactivation location indicated with letter A or A' for the reservoir and B or B' for the basement section of the fault.

footwall injection of a conduit-barrier reverse fault and for sealing and conduit faults that were conducted but are not discussed here in detail for brevity. We find that reactivation in the basement is a characteristic of conductive faults (conduit and conduit-barrier faults) in normal and strike-slip stress regimes regardless of injector location. Conductive faults in reverse faulting regimes and sealing faults in all stress regimes reactivate in the reservoir. For faults that are hydraulically conductive, and regardless of the location of injection into the foot or hanging wall, the direct pressure effect Δp on CFS dominates over the poroelastic effects; among the poroelastic effects, induced changes in normal stress $\Delta\sigma_n$ dominate over induced changes in shear stress $\Delta\tau$ (Figures 5a–5d). In all modeled scenarios that lead to basement fault reactivation, reactivation occurs along the upper basement fault segment (Points B or B'), with no reactivation predicted along the lower basement fault segment (Points C or C') under any of the modeled scenarios.

3.4. Effect of Reservoir-Basement Material Contrast on Fault Reactivation

The simulations so far assumed a higher Young's modulus and Poisson ratio and lower Biot and Skempton coefficients in the basement compared to the reservoir, consistent with reported values (Table 1; Paterson & Wong, 2005; Wang, 2000). To explore the effects of poroelastic coupling parameters on fault reactivation potential, we simulated fluid injection for a conduit-barrier fault in a normal faulting stress regime using the same Biot and Skempton coefficients ($\alpha = 0.44$, $B = 0.46$) in both reservoir and basement, with the other properties as listed in Table 1. Basement fault reactivation is still favored when fluid is injected into the hanging wall side of the fault (Figures 7a and 7b), with reactivation occurring in the basement a few days before the reservoir, whereas reservoir fault reactivation is favored when fluid is injected into the footwall (Figures 7c, 7d, and Table S2). Comparison of these results to those in sections 3.1–3.3 with different poroelastic coupling parameters for basement and sediment (Figures 5a–5d) indicates that an increase in reservoir Biot coefficient increases induced normal stress and decreases induced CFS. For example, the maximum change in CFS resulting from a change in normal stress at point A' for injection into the footwall is -0.39 MPa for $\alpha = 0.79$ (green line in Figure 5c) and -0.2 MPa for $\alpha = 0.44$ (green line in Figure 7c). The depth of fault reactivation is thus dependent on the contrast in poroelastic coupling parameters between reservoir and basement.

4. Discussion

Although frequently ignored in the assessment of fault reactivation in response to fluid injection (Hornbach et al., 2015; Keranen et al., 2013; Lund Snee & Zoback, 2016; Shirzaei et al., 2016), our simulations demonstrate, in agreement with Chang and Segall (2016a, 2016b), that poroelastic stress changes, in combination with the direct pore pressure increase, are controlling if fault reactivation following fluid injection into sedimentary reservoirs occurs in the basement or in the sedimentary reservoir. Although the direct pore pressure

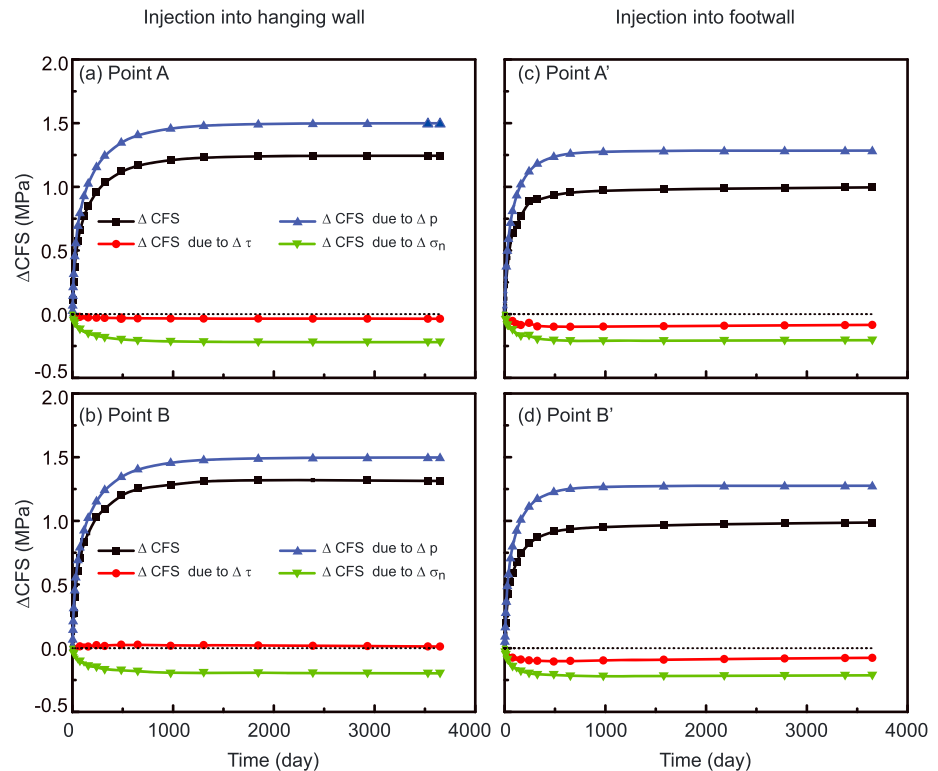


Figure 7. Injection with reservoir and basement having same Biot and Skempton coefficients of 0.44 and 0.46, respectively, for a conduit-barrier fault in a normal faulting stress regime. Changes in CFS due to changes in Δp , τ , and σ_n for injection into the hanging wall (left column, a, b) and footwall (right column, c, d). CFS = Coulomb failure stress.

change exceeds the poroelastic stress in magnitude (Figure 4), pore pressure change alone is not sufficient to account for basement fault reactivation because the direct pressure effect alone (blue lines in Figure 4) would always lead to fault reactivation in the sedimentary layer over the basement (compare blue lines in left column of Figure 4 against right column). It is only in combination with the poroelastic stress component (purple line in Figure 4) that the CFS (black line) is higher in the basement than in the sedimentary layer in the four cases depicted in Figure 6: normal conduit-barrier fault and conduit fault and strike-slip conduit-barrier fault and conduit fault.

In addition to changing fault tractions as described above, the poroelastic stress front propagates beyond the fluid pressurized region. Far from the injector, the poroelastic stress plays a dominant role whereas direct pore pressure changes are confined to the reservoir and the fault damage zone. In contrast to the simulations of Chang and Segall (2016a) that did not consider the effect of the fault on the pressure distribution in the reservoir, we find that fault reactivation in the reservoir is favored over basement for a sealing fault extending from the basement into the reservoir in the normal faulting stress regime. The depth of fault reactivation is dependent on the contrast in poroelastic material constants between reservoir and basement but is generally independent of the location of injection (footwall versus hanging wall) for normal and reverse faults. Compared to the two-dimensional plane strain analysis in Chang and Segall (2016a), the three-dimensional approach followed in the current paper captures the pore pressure gradient and resulting deformation along the fault-strike direction, yielding a better estimate of volumetric expansion of the reservoir associated with fluid injection. The 2-D plane strain analysis tends to overestimate the pore pressure perturbation and the onset of fault reactivation.

Our base-case simulations assume a fault that acts as a barrier to cross-fault flow and as a conduit for flow along the fault in a fractured fault damage zone (conduit-barrier model of Caine et al., 1996). This fault permeability structure is common to many faults containing a fault core composed of consolidated and cemented cataclasite or gouge, fault mineral cement, or entrained shale (Bense et al., 2013; Caine et al., 1996; Knipe, 1992; Vrolijk et al., 2016). Fault-permeability structures are diverse, however, controlled by a

variety of parameters that include host-rock lithology, fault geometry, slip vector magnitude and orientation, stratigraphic juxtaposition, and diagenetic reactions (Bense et al., 2013; Eichhubl et al., 2005). Faults can be barriers to flow without a fault damage zone providing preferred conduits for fault parallel flow (Antonellini & Aydin, 1994; Eichhubl et al., 2009). We have shown that, in the absence of preferred fault-parallel flow conduits, transmission of wastewater into basement is restricted or inhibited and a direct pore pressure effect in the basement excluded, favoring fault reactivation in the reservoir. Poroelastic stresses may still be transmitted from the reservoir into the basement, however, and affect fault stability (Chang & Segall, 2016a). Faults composed of hydraulically conductive opening-mode fractures and sheared fractures may lack a low-permeability fault core and thus act as preferred conduits for flow along the fault while not significantly affecting flow across the fault (transparent to fault-perpendicular flow). Such conduit faults are expected in homogeneous and compositionally and diagenetically mature sandstones (Laubach et al., 2014) and in crystalline basement rocks deformed under upper-crustal conditions (Caine & Tomusiak, 2003; Martel, 1990). We have shown here that conduit faults behave similarly to the conduit-barrier faults with respect to fault reactivation even though they result in a lower excess pore pressure on the upstream side of the fault, resulting in a delay in fault reactivation relative to the conduit-barrier fault. From the operations point of view, the conduit fault would permit a higher excess pressure and, for otherwise identical reservoir properties, a higher volume of injected fluid, before fault reactivation would occur. The conduit-barrier fault model thus provides a fault permeability structure that we consider most prone to fault reactivation in the basement. In detail, fault architecture and thus flow properties can be complex, with different properties for the reservoir and basement segments of the fault.

Fault reactivation is also controlled by the orientation of the fault relative to the in situ stress. We considered faults that are most favorably oriented for each of the three tectonic stress regimes. A less favorable stress orientation would require higher excess pressure for fault reactivation but would not affect relative differences in reactivation potential between reservoir and basement. While it can be generally assumed that most favorably oriented faults are most prone to reactivation (Walsh & Zoback, 2015), unfavorably oriented faults close to the injection well may be reactivated before favorably oriented faults located farther away from the injection (Fan et al., 2016).

Fault reactivation is also controlled by the coefficient of friction (equation (1)). A higher coefficient of friction would delay fault reactivation and allow a higher excess pressure and corresponding higher injection volume before fault reactivation. Conversely, lower fault friction increases the fault reactivation potential.

A review of likely or suggested induced seismic events indicates a prevalence of events in normal and strike-slip faulting stress regimes (Ake et al., 2005; Frohlich et al., 2011, 2016; Horton, 2012; Hornbach et al., 2015; Justinic et al., 2013; Keranen et al., 2013; Kim, 2013; Lund Snee & Zoback, 2016; McNamara et al., 2015; Mousavi et al., 2017; Nicholson et al., 1988; Ogwari et al., 2016; Seeber et al., 2004). Structural heterogeneity, not accounted for in our simulations, can lead to fault behavior that differs from our simulation outcomes. For instance, continuous shale smear or deformation bands in the damage zone may block the pore pressure front from reaching the slip surface of the fault. These structures would only be found in the fault segment that transects the reservoir, thus potentially shielding the reservoir section of the fault from the direct pore pressure effect and favoring fault reactivation in the basement. Variations in fault rock, fault friction, and fault permeability structure along strike and dip could significantly affect the location of fault reactivation and thus reactivation potential of a given fault. While modeling the effects of along-dip and along-strike variations in fault properties are outside the scope of this generic sensitivity analysis, these variations have to be considered in site-specific analyses of fault reactivation potential. Earthquakes have also been associated with water injection in the Western Alberta Basin, Canada, with activity extending from the sedimentary units into the basement (Schultz et al., 2014, 2016). However, the origin of these earthquake sequences in the basement cannot be ascertained.

In this paper we focused on the effects of poroelastic stress, effects of Andersonian stress state, and fault flow properties on basement fault reactivation. Although changes in fault and layer geometry and physical parameters will alter the results of numerical calculations shown here, the main conclusion that stress regime and fault permeability structure affect basement fault reactivation will still hold. For example, increases in the distance between injector and fault, in permeability of reservoir layer, or in the thickness of the reservoir would all result in a lower pore pressure perturbation and thus delay fault reactivation, which can be

explained as follows. The rate of pore pressure front propagation in a poroelastic medium is governed by the hydraulic diffusivity of the fluid-saturated rock D , defined as $D = k/(\mu S)$, with k , μ , and S denoting permeability, fluid viscosity, and storage coefficient, respectively. Hydraulic diffusivity, which is directly proportional to the permeability k and inversely proportional to the storage coefficient S , quantifies the ratio between fluid transport and storage. Increases in permeability of the reservoir layer or in the thickness of the reservoir cause an increase in transmissivity which is the product of hydraulic conductivity and reservoir thickness. The delay in fault reactivation is controlled by the characteristic fluid diffusion time, given by $t = L^2/D$, where L is the characteristic length. Reducing the contrast in permeability between reservoir and basement layers will cause a smaller pore pressure buildup and delay fault reactivation. The effect of increasing the Biot coefficient α is evident from equation (4) predicting an increase in σ_{Hmax} and σ_{hmin} that would result in a smaller differential stress and thus in lower fault reactivation potential in the reservoir in the normal faulting stress regime and in a larger differential stress and a higher fault reactivation potential in the reverse faulting regime.

The response of particular faults, or of fault populations, in specific injection scenarios depends on a wide range of site-specific parameters that include fault and injection well geometry, reservoir and fault flow and mechanical properties, and injection rate and volume, among others. A geomechanical assessment of a specific injection scenario requires a careful and detailed site-specific reservoir flow and geomechanical modeling effort that is beyond the scope of this study and that cannot be replaced with a generic model as provided here. It is the purpose of a generic parametric simulation to shed light on the sensitivity of results to the change of model parameters such as the Andersonian stress state that are not variable at a given site, thus providing wider physical insight and guidance for site-specific simulations.

5. Conclusions

In this paper, we performed a three-dimensional fully coupled poroelastic analysis of basement fault reactivation resulting from fluid injection into overlying sedimentary layer using typical hydromechanical properties for reservoir and basement rocks. We especially focused on the effect of stress regimes, fault permeability structure, poroelastic material contrast between reservoir and basement (Biot and Skempton coefficients), as well as injector location with respect to fault on the basement fault reactivation. Our results highlight the interplay between pore pressure and resulting poroelastic stress and their combined effect on basement fault reactivation for fault-guided fluid flow. The computational framework can be readily generalized to account for more complex site-specific geometry and provide useful guidance for managing and mitigating the risks associated with injection-induced seismicity. The following conclusions can be drawn from our numerical solutions: (1) Reactivation of optimally oriented conduit-barrier and conduit faults in normal faulting stress regimes is favored in basement over reservoir but in reservoir over basement in reverse faulting stress regimes when fluid is injected in the hanging wall. (2) Reactivation of optimally oriented conduit-barrier and conduit faults in strike-slip faulting stress regimes is generally favored in basement over reservoir. (3) Basement fault reactivation in the normal and strike-slip faulting stress regimes is favored because of poroelastic stress changes resulting from the expected contrast in poroelastic properties (Biot and Skempton coefficients) between reservoir and basement. (4) In all simulated scenarios that lead to basement fault reactivation, reactivation occurs along the fault segment in the upper basement; no reactivation is predicted in the lower basement. (5) Sealing faults in all stress regimes reactivate in the reservoir. This finding expands, and is in contrast to, earlier work by Chang and Segall (2016a) who did not extend the fault into the reservoir, thus neglecting the possible effect of the fault on the pressure distribution in the reservoir. (6) For conductive basement faults with direct pore pressure communication with the reservoir (conduit-barrier and conduit faults), the direct pore pressure increase in the conductive fault damage zone prevails over the poroelastic stress in increasing the CFS but is insufficient to account for basement fault reactivation without the coupled poroelastic effects. Geomechanical models without coupled poroelasticity would thus underestimate the basement fault reactivation potential. (7) Among the poroelastic effects, induced normal tractions dominate changes in CFS over induced shear tractions. (8) Combined conduit/barrier faults that are most favorably oriented are most prone to basement fault reactivation. Fault reactivation potential is reduced for conduit faults and faults that are less favorably oriented for slip. (9) Site-specific analyses of fault reactivation potential have to consider along-fault variations in fault frictional and hydraulic properties.

Acknowledgments

We thank the Associate Editor and anonymous reviewers for their helpful comments that greatly improved the paper. This research was conducted under an academic alliance agreement Project No 193418 between Sandia National Laboratories and the University of Texas at Austin and financially supported by the Laboratory Directed Research and Development (LDRD) Program at Sandia National Laboratories and through TexNet. Sandia National Laboratories is a multimission laboratory managed and operated by National Technology and Engineering Solutions of Sandia, LLC., a wholly owned subsidiary of Honeywell International, Inc., for the U.S. Department of Energy's National Nuclear Security Administration under contract DE-NA-0003525. All data used in this study are included in the text. Publication authorized by the Director, Bureau of Economic Geology.

References

- ABAQUS (2014). Abaqus user's guide and help documentation, Version 6.14, SIMULIA Company, Providence.
- Ake, J., Mahrer, K., O'Connell, D., & Block, L. (2005). Deep injection and closely monitored induced seismicity at Paradox Valley, Colorado. *Bulletin of the Seismological Society of America*, 95(2), 664–683. <https://doi.org/10.1785/0120040072>
- Antonellini, M., & Aydin, A. (1994). Effect of faulting on fluid-flow in porous sandstones—Petrophysical properties. *AAPG Bull.*, 78(3), 355–377.
- Barbour, A. J., Norbeck, J. N., & Rubinstein, J. L. (2017). The effects of varying injection rates in Osage county, Oklahoma on the 2016 M 5.8 Pawnee earthquake. *Seismological Research Letters*, 88(4), 1040–1053. <https://doi.org/10.1785/0220170003>.
- Bense, V. F., Gleeson, Z., Loveless, S. E., Bour, O., & Scibek, J. (2013). Fault zone hydrogeology. *Earth-Science Reviews*, 127, 171–192. <https://doi.org/10.1016/j.earscirev.2013.09.008>
- Caine, J. S., Evans, J. P., & Forster, C. B. (1996). Fault zone architecture and permeability structure. *Geology*, 24(11), 1025–1028. [https://doi.org/10.1130/0091-7613\(1996\)024<1025:FZAAPS>2.3.CO;2](https://doi.org/10.1130/0091-7613(1996)024<1025:FZAAPS>2.3.CO;2)
- Caine, J. S., & Tomusiak, S. R. A. (2003). Brittle structures and their role in controlling porosity and permeability in a complex Precambrian crystalline-rock aquifer system in the Colorado Rocky Mountain Front Range. *Geological Society of America Bulletin*, 115(11), 1410–1424. <https://doi.org/10.1130/b25088.1>
- Cappa, F., & Rutqvist, J. (2011). Modeling of coupled deformation and permeability evolution during fault reactivation induced by deep underground injection of CO₂. *International Journal of Greenhouse Gas Control*, 5(2), 336–346. <https://doi.org/10.1016/j.ijggc.2010.08.005>
- Chang, K. W., & Segall, P. (2016a). Injection-induced seismicity on basement faults including poroelastic stressing. *Journal of Geophysical Research: Solid Earth*, 121, 2708–2726. <https://doi.org/10.1002/2015JB012561>
- Chang, K. W., & Segall, P. (2016b). Seismicity on basement faults induced by simultaneous fluid injection—Extraction. *Pure and Applied Geophysics*, 173(8), 2621–2636. <https://doi.org/10.1007/s00024-016-1319-7>
- Eichhubl, P., Davatzes, N. C., & Becker, S. P. (2009). Structural and diagenetic control of fluid migration and cementation along the Moab fault, Utah. *AAPG Bulletin*, 93(5), 653–681. <https://doi.org/10.1306/02180908080>
- Eichhubl, P., S. P., D'Onfro, A., Aydin, A. W., & McCarty, D. K. (2005). Structure, petrophysics, and diagenesis of shale entrained along a normal fault at Black Diamond Mines, California—Implications for fault seal. *AAPG Bulletin*, 89(9), 1113–1137. <https://doi.org/10.1306/04220504099>.
- Ellsworth, W. L. (2013). Injection-induced earthquakes. *Science*, 341(6142), 1225942. <https://doi.org/10.1126/science.1225942>
- Engelder, T. (1993). *Stress regimes in the lithosphere*. Princeton Univ. Press, (p. 457). New Jersey: Princeton.
- Fan, Z., Eichhubl, P., & Gale, J. F. W. (2016). Geomechanical analysis of fluid injection and seismic fault slip for the Mw 4.8 Timpson, Texas, earthquake sequence. *Journal of Geophysical Research: Solid Earth*, 121, 2798–2812. <https://doi.org/10.1002/2016JB012821>
- Frohlich, B. C., Deshon, H., Stump, B., Hayward, C., Hornbach, M., & Walter, J. I. (2016). A historical review of induced earthquakes in Texas. *Seismological Research Letters*, 87(4), 1022–1038. <https://doi.org/10.1785/0220160016>
- Frohlich, C., Ellsworth, W., Brown, W. A., Brunt, M., Luetgert, J., MacDonald, T., & Walter, S. (2014). The 17 May 2012 M4.8 earthquake near Timpson, East Texas: An event possibly triggered by fluid injection. *Journal of Geophysical Research: Solid Earth*, 119, 581–593. <https://doi.org/10.1002/2013JB010755>
- Frohlich, C., Hayward, C., Stump, B., & Potter, E. (2011). The Dallas-Fort Worth earthquake sequence: October 2008 through May 2009. *Bulletin of the Seismological Society of America*, 101(1), 327–340. <https://doi.org/10.1785/0120100131>
- Hornbach, M. J., DeShon, H. R., Ellsworth, W. L., Stump, B. W., Hayward, C., Frohlich, C., et al. (2015). Causal factors for seismicity near Azle, Texas. *Nature Communications*, 6(1), 6728. <https://doi.org/10.1038/ncomms7728>
- Horton, S. (2012). Disposal of hydrofracking waste fluid by injection into subsurface aquifers triggers earthquake swarm in central Arkansas with potential for damaging earthquake. *Seismological Research Letters*, 83(2), 250–260. <https://doi.org/10.1785/gssrl.83.2.250>
- Jeanne, P., Guglielmi, Y., Rutqvist, J., Nussbaum, C., & Birkholzer, J. (2018). Permeability variations associated with fault reactivation in a claystone formation investigated by field experiments and numerical simulations. *Journal of Geophysical Research: Solid Earth*, 123, 1694–1710. <https://doi.org/10.1002/2017JB015149>
- Johann, L., Dinske, C., & Shapiro, S. A. (2016). Scaling of seismicity induced by nonlinear fluid-rock interaction after an injection stop. *Journal of Geophysical Research: Solid Earth*, 121, 8154–8174. <https://doi.org/10.1002/2016JB012949>
- Justinic, A. H., Stump, B., Hayward, C., & Frohlich, C. (2013). Analysis of the Cleburne, Texas, earthquake sequence from June 2009 to June 2010. *Bulletin of the Seismological Society of America*, 103(6), 3083–3093. <https://doi.org/10.1785/0120120336>
- Keranen, K. M., Savage, H. M., Abers, G. A., & Cochran, E. S. (2013). Potentially induced earthquakes in Oklahoma, USA: Links between wastewater injection and the 2011 Mw 5.7 earthquake sequence. *Geology*, 41(6), 699–702. <https://doi.org/10.1130/G34045.1>
- Kim, W. Y. (2013). Induced seismicity associated with fluid injection into a deep well in Youngstown, Ohio. *Journal of Geophysical Research: Solid Earth*, 118, 3506–3518. <https://doi.org/10.1002/jgrb.50247>
- Knipe, R. (1992). Faulting processes and fault seal. In H. B. R. M. Larsen, B. T. Larsen, & E. Talleraas (Eds.), *Structural and tectonic modelling and its application to petroleum geology: Proceedings of Norwegian Petroleum Society Workshop, 18-20 October 1989* (pp. 325–342). Norway: Stavanger. <https://doi.org/10.1016/B978-0-444-88607-1.50027-9>
- Konstantinovskaya, E., Rutqvist, J., & Malo, M. (2014). CO₂ storage and potential fault instability in the St. Lawrence Lowlands sedimentary basin (Quebec, Canada): Insights from coupled reservoir-geomechanical modeling. *International Journal of Greenhouse Gas Control*, 22, 88–110. <https://doi.org/10.1016/j.ijggc.2013.12.008>
- Langenbruch, C., Weingarten, M., & Zoback, M. D. (2018). Physics-based forecasting of man-made earthquake hazards in Oklahoma and Kansas. *Nature Communications*, 9(1), 3946. <https://doi.org/10.1038/s41467-018-06167-4>
- Laubach, S. E., Eichhubl, P., Hargrove, P., Ellis, M. A., & Hooker, J. N. (2014). Fault core and damage zone fracture attributes vary along strike owing to interaction of fracture growth, quartz accumulation, and differing sandstone composition. *Journal of Structural Geology*, 68(Part A), 207–226. <https://doi.org/10.1016/j.jsg.2014.08.007>
- Lund Sneek, J.-E., & Zoback, M. D. (2016). State of stress in Texas: Implications for induced seismicity. *Geophysical Research Letters*, 43, 10,208–10,214. <https://doi.org/10.1002/2016GL070974>
- Martel, S. J. (1990). Formation of compound strike-slip fault zones, Mount Abbot quadrangle, California. *Journal of Structural Geology*, 12(7), 869–882. [https://doi.org/10.1016/0191-8141\(90\)90060-C](https://doi.org/10.1016/0191-8141(90)90060-C)
- McNamara, D. E., Benz, H. M., Herrmann, R. B., Bergman, E. A., Earle, P., Holland, A., et al. (2015). Earthquake hypocenters and focal mechanisms in central Oklahoma reveal a complex system of reactivated subsurface strike-slip faulting. *Geophysical Research Letters*, 42, 2742–2749. <https://doi.org/10.1002/2014GL062730>

- Mousavi, S. M., Ogwari, P. O., Horton, S. P., & Langston, C. A. (2017). Spatio-temporal evolution of frequency-magnitude distribution and seismic index during initiation of induced seismicity at Guy-Greenbrier, Arkansas. *Physics of the Earth and Planetary Interiors*, 267, 53–66. <https://doi.org/10.1016/j.pepi.2017.04.005>
- Nicholson, C., Roeloffs, E., & Wesson, R. L. (1988). The northeastern Ohio earthquake of 31 January 1986: Was it induced? *Bulletin of the Seismological Society of America*, 78, 188–217.
- Nicholson, C., & Wesson, R. L. (1990). Earthquake hazard associated with deep well injection: A report to the U.S. Environmental Protection Agency, Tech. Rep., U.S. Geol. Surv. Bull., Reston, Va.
- Ogwari, P. O., DeShon, H. R., & Hornbach, M. J. (2018). The Dallas-Fort Worth airport earthquake sequence: Seismicity beyond injection period. *Journal of Geophysical Research: Solid Earth*, 123, 553–563. <https://doi.org/10.1002/2017JB015003>
- Ogwari, P. O., Horton, S. P., & Ausbrooks, S. (2016). Characteristics of induced/triggered earthquakes during the startup phase of the Guy-Greenbrier earthquake sequence in North-Central Arkansas. *Seismological Research Letters*, 87(3), 620–630. <https://doi.org/10.1785/0220150252>
- Paterson, M. S., & Wong, T.-f. (2005). *Experimental rock deformation—the brittle field* (2nd ed., 347 pp.). Berlin: Springer.
- Rutqvist, J., Birkholzer, J., Cappa, F., & Tsang, C. F. (2007). Estimating maximum sustainable injection pressure during geological sequestration of CO₂ using coupled fluid flow and geomechanical fault-slip analysis. *Energy Conversion and Management*, 48(6), 1798–1807. <https://doi.org/10.1016/j.enconman.2007.01.021>
- Schultz, R., Corlett, H., Haug, K., Kocou, K., MacCormack, K., Stern, V., & Shipman, T. (2016). Linking fossil reefs with earthquakes: Geologic insight to where induced seismicity occurs in Alberta. *Geophysical Research Letters*, 43, 2534–2542. <https://doi.org/10.1002/2015GL067514>
- Schultz, R., Stern, V., & Gu, Y. J. (2014). An investigation of seismicity clustered near the Cordell Field, west central Alberta, and its relation to a nearby disposal well. *Journal of Geophysical Research: Solid Earth*, 119, 3410–3423. <https://doi.org/10.1002/2013JB010836>
- Seeber, L., & Armbruster, J. G. (1993). Natural and induced seismicity in the Lake Erie-Lake Ontario region: Reactivation of ancient faults with little neotectonic displacement. *Geographie Physique Quaternaire*, 47(3), 363–378.
- Seeber, L., Armbruster, J. G., & Kim, W. Y. (2004). A fluid injection-triggered earthquake sequence in Ashtabula, Ohio: Implications for seismogenesis in stable continental regions. *Bulletin of the Seismological Society of America*, 94(1), 76–87. <https://doi.org/10.1785/0120020091>
- Segall, P., & Fitzgerald, S. D. (1998). A note on induced stress changes in hydrocarbon and geothermal reservoirs. *Tectonophysics*, 289(1–3), 117–128. [https://doi.org/10.1016/S0040-1951\(97\)00311-9](https://doi.org/10.1016/S0040-1951(97)00311-9)
- Segall, P., & Lu, S. (2015). Injection-induced seismicity: Poroelastic and earthquake nucleation effects. *Journal of Geophysical Research: Solid Earth*, 120, 5082–5103. <https://doi.org/10.1002/2015JB012060>
- Shirzaei, M., Ellsworth, W. L., Tiampo, K. F., González, P. J., & Manga, M. (2016). Surface uplift and time-dependent seismic hazard due to fluid injection in eastern Texas. *Science*, 353(6306), 1416–1419. <https://doi.org/10.1126/science.aag0262>
- Tan, X., Konietzky, H., & Frühwirth, T. (2015). Experimental and numerical study on evolution of Biot's coefficient during failure process for brittle rocks. *Rock Mechanics and Rock Engineering*, 48(3), 1289–1296. <https://doi.org/10.1007/s00603-014-0618-5>
- Vrolijk, P. J., Urai, J. L., & Kettermann, M. (2016). Clay smear: Review of mechanisms and applications. *Journal of Structural Geology*, 86, 95–152. <https://doi.org/10.1016/j.jsg.2015.09.006>
- Walsh, F. R., & Zoback, M. D. (2015). Oklahoma's recent earthquakes and saltwater disposal. *Science Advances*, 1(5), e1500195. <https://doi.org/10.1126/sciadv.1500195>
- Wang, H. (2000). *Theory of linear poroelasticity with applications to geomechanics and hydrogeology*. Princeton, N. J: Princeton Univ. Press.
- Yeck, W. L., Weingarten, M., Benz, H. M., McNamara, D. E., Bergman, E. A., Herrmann, R. B., et al. (2016). Far-field pressurization likely caused one of the largest injection induced earthquakes by reactivating a large preexisting basement fault structure. *Geophysical Research Letters*, 43, 10,198–110,207. <https://doi.org/10.1002/2016GL070861>
- Zhai, G., & Shirzaei, M. (2018). Fluid injection and time-dependent seismic hazard in the Barnett Shale, Texas. *Geophysical Research Letters*, 45, 4743–4753. <https://doi.org/10.1029/2018GL077696>
- Zhang, Y., Person, M., Rupp, J., Ellett, K., Celia, M. A., Gable, C. W., et al. (2013). Hydrogeologic controls on induced seismicity in crystalline basement rocks due to fluid injection into basal reservoirs. *Groundwater*, 51(4), 525–538. <https://doi.org/10.1111/gwat.12071>
- Zimmerman, R. W. (2000). Coupling in poroelasticity and thermoelasticity. *International Journal of Rock Mechanics and Mining Sciences*, 37(1–2), 79–87. [https://doi.org/10.1016/S1365-1609\(99\)00094-5](https://doi.org/10.1016/S1365-1609(99)00094-5)